

This is the accepted manuscript made available via CHORUS. The article has been published as:

# Incommensurate dynamic correlations in the quasi-two-dimensional spin liquid $\text{BiCu}_{2}\text{PO}_{6}$

K. W. Plumb, Zahra Yamani, M. Matsuda, G. J. Shu, B. Koteswararao, F. C. Chou, and Young-June Kim

Phys. Rev. B **88**, 024402 — Published 2 July 2013

DOI: [10.1103/PhysRevB.88.024402](https://doi.org/10.1103/PhysRevB.88.024402)

# Incommensurate dynamic correlations in the quasi-two-dimensional spin liquid $\text{BiCu}_2\text{PO}_6$

K.W. Plumb,<sup>1,\*</sup> Zahra Yamani,<sup>2</sup> M. Matsuda,<sup>3</sup> G. J. Shu,<sup>4</sup> B. Koteswararao,<sup>4</sup> F.C. Chou,<sup>4</sup> and Young-June Kim<sup>1,†</sup>

<sup>1</sup>*Department of Physics, University of Toronto, Toronto, Ontario M5S 1A7, Canada*

<sup>2</sup>*Canadian Neutron Beam Centre, National Research Council,  
Chalk River Laboratories, Chalk River, Ontario, K0J 1P0, Canada*

<sup>3</sup>*Quantum Condensed Matter Division, Oak Ridge National Laboratory, Oak Ridge Tennessee 37831, USA*

<sup>4</sup>*Center for Condensed Matter Sciences, National Taiwan University, Taipei, 10617 Taiwan*

(Dated: June 12, 2013)

We report detailed inelastic neutron scattering measurements on single crystals of the frustrated two-leg ladder  $\text{BiCu}_2\text{PO}_6$ , whose ground state is described as a spin liquid phase with no long-range order down to 6 K. Two branches of steeply dispersing long-lived spin excitations are observed with excitation gaps of  $\Delta_1 = 1.90(9)$  meV and  $\Delta_2 = 3.95(8)$  meV. Significant frustrating next-nearest neighbor interactions along the ladder leg drive the minimum of each excitation branch to incommensurate wavevectors  $\zeta_1 = 0.574\pi$  and  $\zeta_2 = 0.553\pi$  for the lower and upper energy branches respectively. The temperature dependence of the excitation spectrum near the gap energy is consistent with thermal activation into singly and doubly degenerate excited states. The observed magnetic excitation spectrum as well as earlier thermodynamic data could be consistently explained by the presence of strong anisotropic interactions in the ground state Hamiltonian.

PACS numbers: 75.10.Jm, 75.10.Kt, 75.40.Gb

## I. INTRODUCTION

Low-dimensional quantum antiferromagnets can realize a rich and diverse array of physical phenomena from a seemingly simple set of interactions. The canonical low-dimensional quantum antiferromagnet is the spin-1/2 Heisenberg chain, in which neighboring spins are coupled with antiferromagnetic exchange  $J_1$ . The system does not have any long range order and the spin-spin correlations decay with a power law. In spin-1/2 chains the elementary excitations are  $S = 1/2$  quasiparticles termed spinons and the dynamic susceptibility is dominated by a gapless dispersive continuum.<sup>1,2</sup> Frustration can be introduced to the spin-1/2 chain by a competing antiferromagnetic next-nearest-neighbor (NNN) interaction  $J_2$ . For a large NNN exchange of  $J_2/J_1 > 0.241$  the ground state is composed of dimerized singlets<sup>3,4</sup> and the excitation spectrum is described as a coherent triplet band of gapped excitations. At the Majumdar-Ghosh (MG) point  $J_2/J_1 = 0.5$  the singlet ground state is exact and the system forms a one-dimensional dimer crystal.<sup>5</sup> As the NNN exchange is increased beyond the MG point frustration drives the spin correlations in the dimerized system to an incommensurate wavevector.<sup>6,7</sup>

A gap may also be introduced into the excitation spectrum by coupling two neighboring chains via a short range interaction  $J_{\text{rung}}$ , to create an even leg ladder.<sup>8</sup> The rung coupling confines spinons into  $S=1$  magnons and the low energy dynamic susceptibility exhibits a well defined, triply degenerate, single particle peak.<sup>9</sup> Theoretical understanding of the properties of even-leg ladders is highly developed<sup>9–11</sup> and a number of experimental realizations have allowed for a detailed understanding of the very rich physical phenomena present in spin-ladders for both the strong rung coupling (rung-singlet)<sup>12–14</sup> and

strong-leg coupling (Haldane)<sup>15,16</sup> regimes. However, the physics of spin ladders with additional frustrating NNN interactions is not understood well. Field theoretical and numerical investigations have indicated that the addition of frustration can lead to many exotic quantum ground states not realized in the standard two-leg ladder,<sup>17–19</sup> yet comprehensive experimental investigations are still lacking.

Such a frustrated two-leg ladder seems to be realized in a newly discovered quasi-two-dimensional spin-1/2 compound  $\text{BiCu}_2\text{PO}_6$ .<sup>20–22</sup> The crystal structure of  $\text{BiCu}_2\text{PO}_6$  is shown in Fig. 1. Zig-zag chains of  $\text{Cu}^{2+}$  ions run parallel to the crystallographic b-axis, as shown clearly by a projection in the **a**–**b** plane in Fig. 1 (c). Along the chains  $\text{Cu}^{2+}$  ions at crystallographically inequivalent sites, labeled  $\text{Cu}_A$  and  $\text{Cu}_B$ , interact via NN antiferromagnetic exchange  $J_1$  and NNN antiferromagnetic exchange  $J_2$  ( $J_1, J_2 > 0$ ). The chains are coupled along the c-axis by both  $J_3$  and  $J_4$ . Although the  $J_3$  interaction distance is shorter than  $J_4$ , band structure calculations predict  $J_4$  to be the dominant coupling along the c-axis.<sup>24</sup> Structurally, this is a result of the particular superexchange pathways.  $J_3$  is a nearly 90° Cu–O–Cu bond, which is usually small and ferromagnetic, in contrast  $J_4$  is mediated by a nearly 180° Cu–O–O–Cu bond. Therefore,  $\text{BiCu}_2\text{PO}_6$  can be considered as a system of  $J_1$ – $J_2$ – $J_4$  ladders with a weaker interladder coupling  $J_3$ .<sup>21,24</sup>

Magnetic susceptibility, magnetization, and heat capacity measurements on powder samples have consistently reported that  $\text{BiCu}_2\text{PO}_6$  has a singlet ground state with a spin excitation gap of  $\sim 2.9$  meV.<sup>20,23–25</sup> The thermodynamic measurements cannot be interpreted in terms of simple gapped one-dimensional (1D) models, including the  $J_1$ – $J_2$  chain and the two-leg ladder,

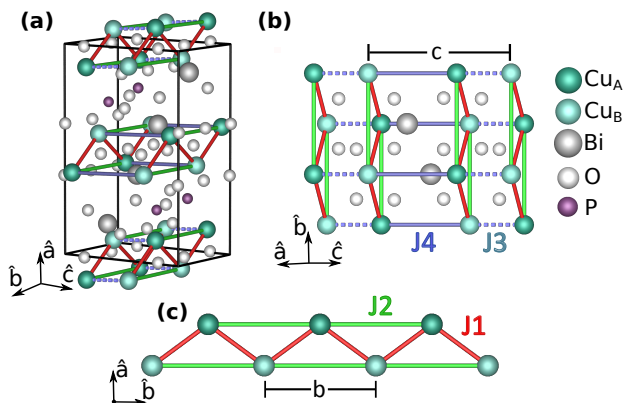


FIG. 1. (a) Schematic representation of the crystal structure of  $\text{BiCu}_2\text{PO}_6$ . The unit cell is orthorhombic, space group  $Pnma$  with  $a = 11.755 \text{ \AA}$ ,  $b = 5.16 \text{ \AA}$ ,  $c = 7.79 \text{ \AA}$  at 6 K.<sup>23</sup> (b) Perspective view of the ladder unit in the  $b$ - $c$  plane and (c) projection into the  $a$ - $c$  plane showing the zigzag chains of  $\text{Cu}^{2+}$  ions.

but require a combination of frustration and two-leg-ladder geometry.<sup>21,25</sup> Inelastic neutron scattering (INS) measurements on powder samples have reported that  $\text{BiCu}_2\text{PO}_6$  has a dispersive spin excitation spectrum with a gap of  $\Delta = 2.9 \text{ meV}$  and that significant frustration is required to describe the powder averaged structure factor.<sup>21</sup> More recent high field magnetization measurements on single crystals have revealed that the critical field for the closing of the spin gap is dependent on the direction of the applied field indicative of strong anisotropic interactions in the magnetic Hamiltonian.<sup>26</sup>

In real materials (usually) small anisotropic interactions, in addition to the Heisenberg exchange couplings, invariably exist. Such interactions are often a negligible perturbation to the isotropic Heisenberg interaction, as in cuprate superconductors,<sup>27,28</sup> but can sometimes alter the magnetic properties in a fundamental way. As an example, for compounds that lack local inversion symmetries anisotropic Dzyaloshinsky-Moriya (DM)<sup>29,30</sup> interactions are permitted in the magnetic Hamiltonian. Depending on the particular crystallographic symmetries the DM interaction can induce a staggered field.<sup>31</sup> In 1D chains this staggered field results in an effective confinement potential between spinons and the appearance of incommensurate gapped modes on application of a magnetic field.<sup>31–33</sup> The staggered field also has a drastic effect for spin ladders. In contrast to a spin ladder in a uniform magnetic field, which transitions to a gapless phase above a critical field, the presence of a staggered field is predicted to lead to a quantum phase transition between two gapped phases above and below the critical field.<sup>34</sup>

The numerous exchange pathways in  $\text{BiCu}_2\text{PO}_6$  complicate interpretation of thermodynamic data and important details including interladder coupling and anisotropic interactions are often neglected in the analysis. In order to determine the microscopic

spin Hamiltonian of a complex magnetic system with competing interactions and anisotropic exchange couplings, INS measurements using a single crystal sample are essential.

We have conducted an extensive neutron scattering study of the magnetic excitation spectrum in  $\text{BiCu}_2\text{PO}_6$ . Our data confirms that  $\text{BiCu}_2\text{PO}_6$  is appropriately described by weakly interacting two-leg ladders with incommensurate dynamic correlations driven by frustration. In contrast to the single triply degenerate excitation branch expected for an isotropic ladder, we observe two branches of steeply dispersing, long-lived, excitations. The excitation gap of each mode, directly probed by INS, was measured to be  $\Delta_1 = 1.90(9) \text{ meV}$  and  $\Delta_2 = 3.95(8) \text{ meV}$ , this differs significantly from the  $\sim 2.9 \text{ meV}$  gap extracted from thermodynamic measurements<sup>20,23,24</sup> indicating that current models are inadequate to describe the ground state of  $\text{BiCu}_2\text{PO}_6$ . Furthermore, the temperature dependence of the incommensurate modes are consistent with a description in terms of thermal activation into singly and doubly degenerate modes. We argue that, in addition to frustration, strong anisotropic interactions are important for understanding the physics of this material.

## II. EXPERIMENTAL DETAILS

Experiments were carried out on a 4.5 g single crystal sample grown using the traveling floating zone method. The sample mosaic was measured by neutron scattering to be  $0.2^\circ$  at  $T = 6 \text{ K}$ . Measurements were performed on the C5 DUALSPEC triple axis spectrometer at the Canadian Neutron Beam Centre at Chalk River Laboratories and on the HB1 triple axis spectrometer at HFIR. Both instruments employed a vertically focusing pyrolytic graphite (PG) monochromator and C5 was equipped with a flat graphite analyzer while HB1 utilized a fixed vertically focusing analyzer. On C5 the sample was mounted in the  $(0, k, l)$  scattering plane and the spectrometer was operated at a fixed final energy of  $14.56 \text{ meV}$ . Experiments on HB1 were performed with the sample mounted in both the  $(h, k, 2k)$  and  $(0, k, 1)$  horizontal scattering planes at a fixed final energy of  $14.7 \text{ meV}$ . Temperature control was provided by a closed cycle cryostat. All data was corrected for higher-order wavelength neutrons in the incident beam monitor.<sup>35</sup> Intensities were placed on an absolute scale by normalization with the integrated intensity of a transverse acoustic phonon measured near the  $(004)$  Bragg peak on the respective instrument.

The crystallographic unit cell of  $\text{BiCu}_2\text{PO}_6$  is orthorhombic, space group  $Pnma$  with  $a = 11.755 \text{ \AA}$ ,  $b = 5.16 \text{ \AA}$ ,  $c = 7.79 \text{ \AA}$ . Along the zig-zag chains NN  $\text{Cu}^{2+}$  ions in  $\text{BiCu}_2\text{PO}_6$  are separated by  $b/2$  so that the momentum of magnetic excitations in the  $\mathbf{b}^*$  direction is indexed using  $\bar{\mathbf{k}} = \mathbf{q} \cdot \mathbf{b}/2 = \pi \mathbf{k}$ .

### III. EXPERIMENTAL RESULTS

#### A. Spin excitation spectra

The momentum and energy dependence of spin excitations in  $\text{BiCu}_2\text{PO}_6$  were surveyed through a series of constant- $\mathbf{Q}$  and constant energy transfer scans. No evidence for elastic magnetic scattering at  $T = 6$  K was found indicating the absence of static magnetic correlations in  $\text{BiCu}_2\text{PO}_6$ . Representative scans taken in proximity of the spin gap at  $T = 6$  K are shown in Fig. 2. Throughout most of the Brillouin zone the scattering in-

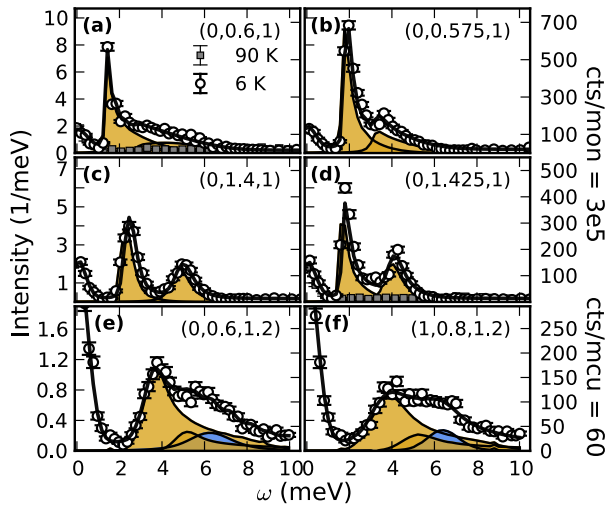


FIG. 2. Representative constant- $\mathbf{Q}$  scans. Data in panels (a)-(d) were obtained on C5 with the sample aligned in the  $(0, k, l)$  scattering plane and a collimation of  $33^\circ\text{-}48^\circ\text{-}51^\circ\text{-}144^\circ$ . Data in panels (e) and (f) was obtained on HB1 with the sample aligned in the  $(h, k, 2k)$  scattering plan and a collimation of  $48^\circ\text{-}40^\circ\text{-}40^\circ\text{-}120^\circ$ . All data was collected at  $T = 6$  K. The solid black lines are the results of a global fit to the single mode approximation, gold and blue filled areas show the contribution from each mode including resolution effects.

tensity is dominated by two well defined modes which are highly dispersive near the minimum of the excitation spectra. The dispersion of these modes is not commensurate with the structural unit cell and the scattering intensity vanishes as the temperature is increased above 60 K, where a broad maxima in the magnetic susceptibility was observed,<sup>20</sup> confirming the magnetic origin.

Constant energy transfer scans detailing the inelastic scattering in the neighbourhood of the incommensurate wavevector are shown in Fig. 3. These scans highlight the incommensurate dynamic correlations in  $\text{BiCu}_2\text{PO}_6$  and the highly dispersive nature of the low energy excitations. Below the gap the inelastic signal decreases to background, while at the gap energy the dynamic correlations give rise to a resolution limited signal, centered on an incommensurate wavevector, Fig. 3 (b).

Extensive sampling of  $\mathbf{Q}$ -values throughout reciprocal space enabled the construction of a map of the

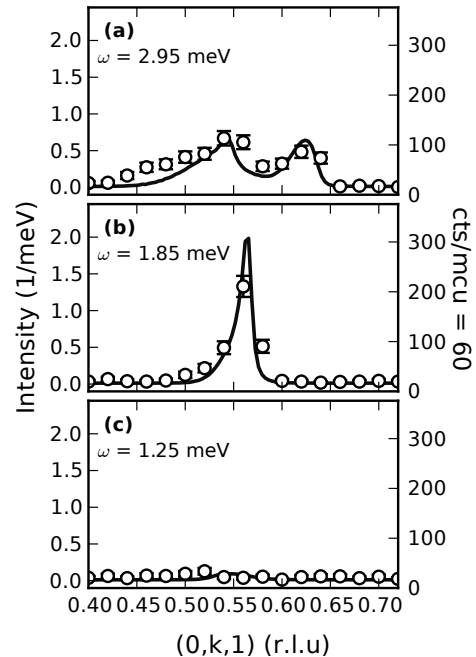


FIG. 3. Constant energy transfer scans around the gap energy. Data was obtained on HB1 with a collimation of  $48^\circ\text{-}20^\circ\text{-}20^\circ\text{-}60^\circ$ . All data was collected at  $T = 6$  K. The solid black lines are the results of a global fit to the single mode approximation.

dynamic structure factor  $S(\mathbf{q}, \omega)$  shown in Fig. 4 (a) - (c). Magnetic excitations in  $\text{BiCu}_2\text{PO}_6$  are highly anisotropic, with a bandwidth of at least 12 meV in the  $\mathbf{b}^*$  direction and  $\sim 2$  meV in the  $\mathbf{c}^*$  direction. Dispersion along the  $\mathbf{c}^*$  direction confirms the presence of sizable interladder interactions. Any dispersion along the  $\mathbf{a}^*$  direction could not be resolved by our thermal triple axis measurements, indicating that  $\text{BiCu}_2\text{PO}_6$  should be regarded as a quasi-two-dimensional system.

Within the first Brillouin zone, each branch of the excitation spectrum has two minima occurring at wavevectors  $\zeta_\alpha = 0.5 + \delta_\alpha$  and  $\zeta_\alpha = 1.5 - \delta_\alpha$ . The distinct double-well structure is reminiscent of the dispersion in  $J_1$ - $J_2$  chains and the incommensurate minima indicative of a strong competition between  $J_1$  and  $J_2$ .<sup>6,7,17,19</sup>

The excitation spectrum shown in Fig. 4(a) cannot be described using strong-coupling expansions for a two-leg ladder with competing interactions.<sup>19,24</sup> These perturbative expansions require that the rung coupling ( $J_4$ ) is much larger than the coupling along the chains ( $J_1, J_2$ ). However, the large bandwidth of each branch compared with the gap energies implies that  $\text{BiCu}_2\text{PO}_6$  likely lies in an intermediate coupling regime where  $J_1 \sim J_4$ , this is in qualitative agreement with band-structure calculations.<sup>24</sup>

Inelastic neutron scattering directly probes the dynamic spin correlation function convolved with a well-

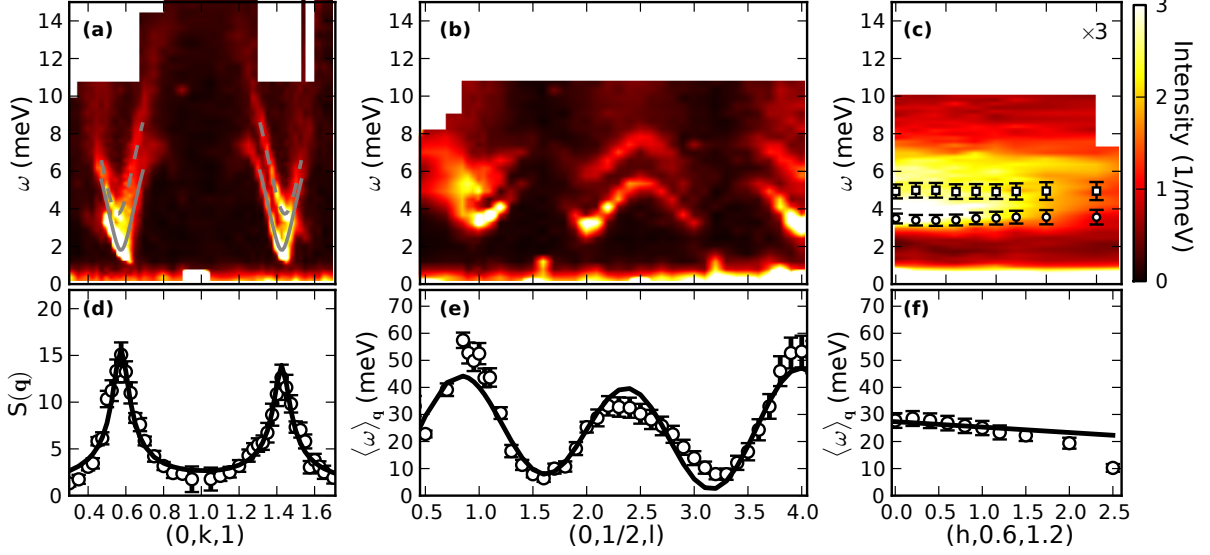


FIG. 4. (a) - (c) Inelastic neutron scattering intensity map for  $T = 6\text{K}$  constructed by linear interpolation of a series of constant scans. All data have been corrected for the isotropic  $\text{Cu}^{2+}$  form factor. Solid and dashed gray lines show the dispersion relation, Eq. (1), using the parameters obtained from the single mode approximation fit. Solid white symbols in (c) show the fitted peak positions of resolution limited mode. (d) Structure factor data obtained at  $T = 6\text{K}$ , for equal-time spin correlations along the chain  $\mathbf{b}^*$  direction, calculated by numerically integrating constant  $\mathbf{q}$  scans for  $\omega > 0.5\text{meV}$ . (e) - (f) Measured first moment as a function of wavevector along the rung  $\mathbf{c}^*$  direction and perpendicular to the planes of the ladders, along  $\mathbf{a}^*$ . Solid lines are fits as described in the text.

defined spectrometer resolution function. As a result of the steep dispersion, and proximity of the two modes, the line shape observed for a given constant momentum transfer scans was drastically affected by the spectrometer resolution. The resolution effects are best illustrated by comparing panel (a) and panel (c) in Fig. 2, which are constant momentum transfer scans taken at equivalent positions in the magnetic Brillouin zone but with different orientations of the spectrometer resolution ellipsoid with respect to the dispersion surface. While the favourable orientation of the resolution ellipsoid at  $\mathbf{Q} = (0, 1.4, 1)$  results in the appearance of two well defined modes, at  $\mathbf{Q} = (0, 0.6, 1)$  the two modes are completely defocused and a broad spectra is observed. In order to extract precise quantitative results from our data it is necessary to fully take into account instrumental resolution effects.

Lacking a microscopically motivated theory for  $\text{BiCu}_2\text{PO}_6$  the essential features of the lowest energy excitations, near the incommensurate wavevector, were determined by fitting data in the vicinity of the dispersion minimum with a single mode approximation (SMA) cross-section including two well-defined modes, and an empirical dispersion relation:

$$(\omega_{\mathbf{q}}^{\alpha})^2 = \Delta_{\alpha}^2 + v_{\alpha}^2 \sin^2(\tilde{k} - \pi\zeta_{\alpha}), \quad (1)$$

$$S(\mathbf{q}, \omega) = \frac{1}{1 - e^{-\omega_{\mathbf{q}}^{\alpha}/T}} \frac{\mathcal{A}_{\mathbf{q}}^{\alpha}}{\omega_{\mathbf{q}}^{\alpha}} \delta(\omega - \omega_{\mathbf{q}}^{\alpha}), \quad (2)$$

$\mathcal{A}_{\mathbf{q}}^{\alpha}$  is a mode dependent intensity pre-factor,  $v_{\alpha}$  param-

eterizes the spin-wave velocity of each mode, and we set  $\hbar = k_B = 1$  throughout this paper. The use of a single mode approximation is justified when the scattering intensity is dominated by one or more well defined resolution limited modes. Equation (2) was convolved with the instrumental resolution function<sup>36,37</sup> and globally fit to scans in the range  $0.5\pi < \tilde{k} < 0.7\pi$  and  $1.3\pi < \tilde{k} < 1.5\pi$ , only  $\mathcal{A}_{\mathbf{q}}^{\alpha}$  was allowed to vary between scans. Incoherent background was modeled as a constant plus a Gaussian function centered on  $\omega = 0$ . The broad peak widths and  $\mathbf{Q}$ -dependence of lineshapes visible in Fig. 2 (a)-(d) and Fig. 4 (a)-(b) are accounted for entirely by resolution effects and two steeply dispersing modes indicating that the excitations are long-lived. Additional intensity appears in  $(h, k, 2k)$  plane which is best accounted for by a damped harmonic oscillator, blue shaded area in Fig. 2 (e) and (f).<sup>38</sup> Dispersion parameters determined from the low-energy global fit were:  $\Delta_1 = 1.90(9)\text{meV}$ ,  $\Delta_2 = 3.95(8)\text{meV}$ ,  $v_1 = 16.4(1.4)\text{meV}$ ,  $v_2 = 19.6(1.7)\text{meV}$ ,  $\delta_1 = 0.074(2)$ ,  $\delta_2 = 0.053(4)$ . Scans simulated using these parameters are shown as solid lines in Fig. 2 and Fig. 3. The resulting dispersion is plotted as solid and broken grey lines in Fig. 4 (a).

Only fluctuations perpendicular to the momentum transfer  $\mathbf{Q}$  will contribute to the neutron scattering cross-section, thus by measuring the relative intensity of each mode at different gap wavevectors we can obtain information on the polarization of each mode after accounting for magnetic form factor and spectrometer resolution effects. Along the  $\mathbf{c}^*$  direction the relative intensity of the upper

and lower branch is constant and neither mode appears to contain a component with significant polarization along this direction. However, for momentum transfers along the  $\mathbf{b}^*$  direction the intensity of the lower branch is decreased by  $\sim 35\%$  between the gap wavevectors at  $\mathbf{Q} = (0, 0.574, 1)$  and  $\mathbf{Q} = (0, 1.426, 1)$ , whereas the intensity of the higher branch is constant. Thus the two modes must have distinct polarizations, with the lower energy mode containing a component that is polarized along the chain  $\mathbf{b}^*$  direction and the upper mode polarized predominantly perpendicular to the planes of the ladders, along the  $\mathbf{a}^*$  direction.

The incommensurate wavevector of the lower branch  $\zeta_1 = 0.574\pi$  can be used to estimate the ratio  $J_2/J_1$  in the two limits of strong rung coupling  $J_4 > J_1$  and uncoupled weakly interacting  $J_1$ - $J_2$  chains. For strong rung coupling the wavevector minimizing the dispersion can be estimated exactly<sup>19</sup>

$$\zeta = \arccos\left(\frac{-J_1}{4J_2}\right), \quad (3)$$

giving  $J_2/J_1 = 1.08$ . In the opposite limit of isolated  $J_1$ - $J_2$  chains, density matrix renormalization group (DMRG) results<sup>7</sup> can be used to estimate  $J_2/J_1$  from  $\zeta$  giving  $J_2/J_1 \approx 0.9$ . Furthermore, using our measured gap value and the  $J_2/J_1$  ratio, the DMRG results predict a nearest-neighbour exchange of  $J_1 = 4\Delta_1 = 7.6$  meV in reasonable agreement with first principles calculations.<sup>24</sup> Our INS data situates  $\text{BiCu}_2\text{PO}_6$  in an intermediate coupling regime; however, the two limits of isolated chains and strong rung coupling tightly constrain  $J_2 \approx J_1$ .

Information about the length scales associated with spin correlations can be extracted from the equal-time structure factor, shown in Fig. 4 (d). It was calculated by numerically integrating constant  $\mathbf{q}$  scans between 0.5 and 15 meV, all scans were corrected for the isotropic  $\text{Cu}^{2+}$  form-factor prior to integration.<sup>39</sup> Static correlations in  $\text{BiCu}_2\text{PO}_6$  are well described by a double peaked square root Lorentzian, characteristic of spin chains with competing NN and NNN interactions and exponentially decaying spin-spin correlations<sup>40</sup>

$$S(k) \propto \frac{1}{\sqrt{\kappa^2 + (k - \zeta')^2}} + \frac{1}{\sqrt{\kappa^2 + (k - \zeta'')^2}}, \quad (4)$$

where  $\zeta' = 0.5 + \delta$ ,  $\zeta'' = 1.5 - \delta$  and  $\xi = 1/\kappa$  is the correlation length. Fitting Eq. (4) to data in Fig. 4 (d) yields a spin-spin correlation length of  $\xi/(b/2) = 8.0(6)$  and  $\delta = 0.074(5)$ .

The  $\sim 2$  meV bandwidth along the  $\mathbf{c}^*$  direction implies that there is a significant coupling between the ladder units. However, it is not possible to distinguish either  $J_3$  or  $J_4$  as the inter/intra ladder coupling from the shape of the dispersion alone. More information is contained in the modulation of INS intensity along the  $\mathbf{c}^*$  and  $\mathbf{a}^*$  directions. In the absence of a microscopic model for the spin dynamics in  $\text{BiCu}_2\text{PO}_6$  the first moment sum

rule can be utilized to determine the relative contribution of spin-pair correlations across each bond to the ground state energy.<sup>41,42</sup> For a Heisenberg Hamiltonian the first moment sum rule is written

$$\begin{aligned} \langle \omega \rangle_{\mathbf{q}} &= \int_{-\infty}^{\infty} \omega S^{\alpha\alpha}(\mathbf{q}, \omega) d\omega \\ &= -\frac{1}{3} \sum_{j,j'} J_{jj'} \langle \mathbf{S}_j \mathbf{S}_{j'} \rangle [1 - \cos(\mathbf{q} \cdot \mathbf{r}_{jj'})], \end{aligned} \quad (5)$$

where  $\langle S_j^\beta S_{j'}^\beta \rangle$  is the spin-spin correlation across bond  $\mathbf{r}_{jj'}$ . Within the single mode approximation the dimer-interference term  $[1 - \cos(\mathbf{q} \cdot \mathbf{r}_{jj'})]$  accounts entirely for the  $\mathbf{q}$ -dependent intensity modulation of the inelastic scattering intensity along the rung direction for a system of isolated ladders.<sup>12,43</sup> However, the sum rule in Eq. (5) is strictly only valid for a centro-symmetric lattice obeying inversion symmetry, hence must be applied with caution when analyzing the spectrum from  $\text{BiCu}_2\text{PO}_6$  where a significant DM anisotropy on each rung is potentially present. The first-moment was measured in  $\text{BiCu}_2\text{PO}_6$  by numerically integrating constant- $\mathbf{q}$  scans along the  $\mathbf{a}^*$  and  $\mathbf{c}^*$  directions and globally fit to equation (5). All scans were corrected for the isotropic  $\text{Cu}^{2+}$  form-factor prior to integration.<sup>39</sup> Intensity modulation along the  $\mathbf{c}^*$  and  $\mathbf{a}^*$  directions is well described including only bonds  $J_3$  and  $J_4$ , with  $J_4 \langle \mathbf{S}_0 \mathbf{S}_4 \rangle / J_3 \langle \mathbf{S}_0 \mathbf{S}_3 \rangle = 4.8$ , results of the fit are shown as solid lines in Fig. 4 (e) - (f). The intensity modulation is thus consistent with a two-leg ladder formed by antiferromagnetic rung coupling  $J_4$  and weaker interladder coupling  $J_3$ .

Our neutron scattering results confirm that the  $J_1$ - $J_2$ - $J_4$  two-leg ladder with interladder exchange  $J_3$  is an appropriate description of  $\text{BiCu}_2\text{PO}_6$ . However, the gap energy differs significantly from the value of  $\Delta \sim 2.9$  meV reported by previous thermodynamic measurements.<sup>20,21,24</sup> This discrepancy is potentially resolved by the presence of strong anisotropic interactions neglected in the thermodynamic analysis. These anisotropies can act to split the degeneracy of the lowest lying excitations in zero field, so that the thermodynamic properties are controlled by two gaps. An anisotropy induced splitting is consistent with the different polarizations of the upper and lower mode. It is notable that the 2.9 meV thermodynamic gap is in agreement with the average of the two gaps measured by INS,  $1/2(\Delta_1 + \Delta_2) = 2.93(6)$  meV. We have also checked that the low-temperature magnetic specific heat can be fit using an effective 1D model including the sum of contributions from both the low and high energy modes  $C_m = 1/2(g_1 \exp(-\Delta_1/T) + g_2 \exp(-\Delta_2/T))$  with each gap fixed at the value determined from INS. Furthermore, a zero-field splitting of the lowest lying excitation resulting from a strong anisotropic interaction is consistent with the temperature dependence data presented next.



## B. Temperature Dependence

The temperature dependence of spin excitations at  $\mathbf{q} = (0, 1.425, 1)$  near the incommensurate wavevector is shown in Fig. 5(a). As the temperature is increased the inelastic features broaden and shift to higher energies. Above 25 K the two excitations can no longer be distinctly identified and above 55 K the inelastic signal cannot be distinguished from background. Each spectrum

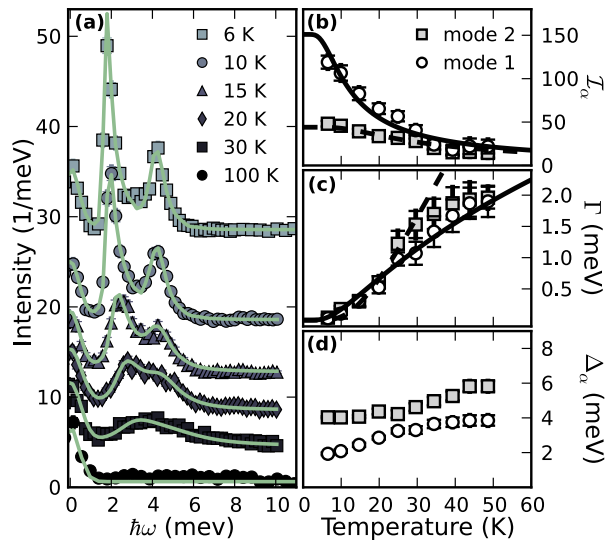


FIG. 5. Temperature dependence of spin excitations near the incommensurate wavevector at  $(0, 1.425, 1)$ , data collected on C5. (a) A series of representative constant- $\mathbf{q}$  scans, data has been offset for clarity, solid lines are fit to resolution convolved cross-section. (b) - (d) Results of fit to resolution convolved Lorentzian scattering cross-section. Solid and dashed lines in (b) are fit to the population thermalization factor from RPA theory. The solid and dashed lines in (c) are a fit to exponential activated behaviour as described in the text.

was fit to the resolution convolved single mode cross section [Eq. (2)] with a normalized Lorentzian function in place of the delta function to account for intrinsic broadening of each mode. Lacking detailed measurements of the dispersion for  $T > 6$  K the spin wave velocity was assumed to be independent of temperature for all fits. Constant- $\mathbf{q}$  scans were performed at a wavevector where the orientation of the resolution ellipsoid with respect to the slope of the dispersion minimizes any resolution effects. We have also checked that allowing for a temperature dependent spin wave velocity does not affect the results presented here. Figures 5 (b) - 5(d) show the temperature dependence of the integrated intensity, half-width half-maximum and gap energy of each mode.

In accordance with the thermalization of the ground and excited states, the integrated intensity decreases with increasing temperature. The random phase approximation (RPA) for weakly interacting dimers predicts the scattering intensity to scale with the ground-state excited-state population difference  $\Delta n(\Delta_\alpha/T) =$

$(1 - \exp(-\Delta_\alpha/T)) / (1 + \eta \exp(-\Delta_\alpha/T))$ , where  $\eta$  is the degeneracy of the level.<sup>44-46</sup> The RPA form is a good description of the data after fitting only an overall scale factor [solid lines in Fig. 5 (b)]. The best fit is obtained assuming the two modes are composed of a lower energy doubly degenerate excitation ( $\Delta_1$ ) and a higher energy singly degenerate excitation ( $\Delta_2$ ). Although we do not have sufficiently detailed data to completely rule out the possibility of two triply degenerate modes. The scaling of the intensities provides good qualitative evidence for the splitting of a single triply degenerate excitation band into a doublet and singly degenerate excitation.

For one-dimensional systems with a gapped excitation spectrum increasing temperature results in an increased density of thermally activated states and concomitantly a decrease in the mean free path between scattering of the excited states, or equivalently a decreased excitation lifetime.<sup>47-49</sup> Thus, we expect a thermally induced broadening of the excitation spectrum, as visible in Fig. 5 (c). Below 30 K the damping is consistent with an exponential activated behaviour  $\Gamma_\alpha = g_\alpha \sqrt{\Delta_\alpha/T} \exp(\Delta_\alpha/T)$ , valid for gapped one-dimensional systems.<sup>47</sup> The fitted scale factors were  $g_1 = 1.05(1)$  and  $g_2 = 2.22(16)$  for the low and high energy modes respectively and the fits are shown as solid and dashed lines in Fig. 5(c). A slight increase in excitation energy with increasing temperature was also observed [Fig. 5 (d)]. This is understood in the context of the thermally induced "blue-shift" that has been reported in other quasi-one-dimensional systems.<sup>48-52</sup> Hence, the magnetic excitations in  $\text{BiCu}_2\text{PO}_6$  are consistent with expectations for one-dimensional gapped quantum spin liquids where the temperature dependence is controlled by interactions between well defined quasi-particles. However, for  $\text{BiCu}_2\text{PO}_6$  two-dimensional interactions are not negligible as evidenced by the 2 meV bandwidth of excitations along the  $\mathbf{c}^*$  direction. This places  $\text{BiCu}_2\text{PO}_6$  in an interesting limit between one and two-dimensional gapped spin-liquid ground states.

## IV. DISCUSSION

The excitation spectrum in  $\text{BiCu}_2\text{PO}_6$  is unique in that competing interactions along the spin chains drive the dynamic correlations to an incommensurate wavevector. The excitation spectrum is reminiscent of the incommensurate correlations that have been observed in other low dimensional systems with competing interactions such as  $\text{LiCu}_2\text{O}_2$ <sup>53,54</sup> and  $\beta\text{-CaCr}_2\text{O}_4$ <sup>55</sup>, however these systems display long-range static order at the incommensurate wavevector, and the excitation spectrum can be explained within the semiclassical-limit using linear spin-wave theory. In contrast, the ground state of  $\text{BiCu}_2\text{PO}_6$  is entirely quantum mechanical, there is no static magnetic order and the incommensurate correlations are entirely dynamic. Incommensurate dynamic correlations have been observed in the four-leg antifer-

romagnetic spin tube  $\text{Sul} - \text{Cu}_2\text{Cl}_4$ <sup>56</sup>; however, the degree of incommensurability was much smaller than that observed in  $\text{BiCu}_2\text{PO}_6$ . Furthermore, the excitations in  $\text{Sul} - \text{Cu}_2\text{Cl}_4$  are comprised of a single, triply degenerate mode, while in  $\text{BiCu}_2\text{PO}_6$  the degeneracy is split and the minimum of each mode occurs at a different wave vector.

In a canonical two-leg ladder the low energy magnetic excitation spectrum is composed of a well defined branch of dispersing triplets. Application of an external magnetic field splits the degeneracy and three branches of excitations may be observed.<sup>15</sup> The degeneracy may also be split in the presence of anisotropic interactions in the microscopic Hamiltonian.<sup>34,57</sup> We believe that the observed mode splitting in  $\text{BiCu}_2\text{PO}_6$  may be accounted for by significant staggered DM interactions. Although the presence of a DM anisotropy in  $\text{BiCu}_2\text{PO}_6$  cannot be concluded from our INS data alone, DM interactions account for many features of the thermodynamic measurements including the weak linear field dependence of the low field magnetization below  $H_c$ ,<sup>24,26</sup> highly anisotropic critical fields,<sup>26</sup> and absence of square root singularity in magnetization just above  $H_c$ .<sup>24,57</sup> In  $\text{BiCu}_2\text{PO}_6$  local inversion symmetry is broken allowing a DM interaction, with the particular crystallographic symmetries admitting a DM anisotropy with a staggered DM vector on each rung as well as DM interactions on the chain bonds.<sup>24</sup> Although there are many possible DM vectors, our INS measurements can only resolve two-bands of excitations in zero-field indicating that the magnetic Hamiltonian retains a local symmetry, so that we expect a single, dominant, anisotropy term. Field theoretical modeling has shown that staggered anisotropic interactions in a spin-1/2 two-leg ladder can act to split the lowest lying triplet into a doublet with energy  $\Delta_d < \Delta_t$  and higher energy mode with  $\Delta_3 > \Delta_t$ .<sup>34</sup> Our temperature dependent measurements are consistent with this scenario, although further detailed magnetic field dependent measurements are required to definitively establish the degeneracy of each mode.

In summary, we have measured the spin excitation spectrum in  $\text{BiCu}_2\text{PO}_6$  at 6 K. We find no evidence for static magnetic correlations confirming that  $\text{BiCu}_2\text{PO}_6$  is in a quantum disordered phase. Furthermore, the  $J_1$ - $J_2$ - $J_4$  two-leg ladder model with interladder exchange  $J_3$  appropriately accounts for the dominant exchange pathways. The measured incommensurate wavevector  $\zeta = 0.574\pi$  allows for an estimate of the relative strength of the competing magnetic interactions  $J_2/J_1 \sim 1$ . However, the lowest excitation gap is 1.90(9), is significantly lower than the value of 2.9 predicted by thermodynamic measurements. The discrepancy may be explained by the presence of strong anisotropic magnetic interactions which split the excitation spectrum into two coherent branches. We hope that our data will stimulate further theoretical work investigating the effect of anisotropic interactions and frustration on the spin-liquid ground state of a even-leg ladder.

## ACKNOWLEDGMENTS

We would like to thank Yong-Baek Kim, Arun Paramakanti, and Leon Balents for useful discussions. Y.J. Kim acknowledges the hospitality and the Aspen Center for Physics supported in part by the National Science Foundation under grant No. PHYS-1066293. Work at the University of Toronto was supported by NSERC of Canada. Work at Chalk River Labs was supported by NSERC of Canada, NRC of Canada. Work at HFIR was sponsored by the Scientific User Facilities Division, Office of Basic Energy Sciences, U.S. Department of Energy. K.W. Plumb acknowledges the support of the Ontario Graduate Scholarship.



- \* kplumb@physics.utoronto.ca  
† yjkim@physics.utoronto.ca
- <sup>1</sup> D. A. Tennant, R. A. Cowley, S. E. Nagler, and A. M. Tsvelik, Phys. Rev. B **52**, 13368 (1995).
  - <sup>2</sup> D. C. Dender, D. Davidović, D. H. Reich, C. Broholm, K. Lefmann, and G. Aeppli, Phys. Rev. B **53**, 2583 (1996).
  - <sup>3</sup> F. D. M. Haldane, Phys. Rev. B **25**, 4925 (1982).
  - <sup>4</sup> K. Okamoto and K. Normura, Phys. Lett. A **169**, 433 (1992).
  - <sup>5</sup> C. K. Majumdar and D. K. Ghosh, J. Math. Phys. **10**, 1388 (1969).
  - <sup>6</sup> R. Bursill, G. A. Gehring, D. J. J. Farnell, J. B. Parkinson, T. Xiang, and C. Zeng, J. Phys. Condens. Matter **7**, 8605 (1995).
  - <sup>7</sup> S. R. White and I. Affleck, Phys. Rev. B **54**, 9862 (1996).
  - <sup>8</sup> E. Dagotto and T. M. Rice, Science **271**, 618 (1996).
  - <sup>9</sup> D. G. Shelton, A. A. Nersesyan, and A. M. Tsvelik, Phys. Rev. B **53**, 8521 (1996).
  - <sup>10</sup> S. Gopalan, T. M. Rice, and M. Sigrist, Phys. Rev. B **49**, 8901 (1994).
  - <sup>11</sup> T. Giamarchi and A. M. Tsvelik, Phys. Rev. B **59**, 11398 (1999).
  - <sup>12</sup> T. Masuda, A. Zheludev, H. Manaka, L. P. Regnault, J. H. Chung, and Y. Qiu, Phys. Rev. Lett. **96**, 047210 (2006).
  - <sup>13</sup> V. O. Garlea, A. Zheludev, T. Masuda, H. Manaka, L. P. Regnault, E. Ressouche, B. Grenier, J. H. Chung, Y. Qiu, K. Habicht, K. Kiefer, and M. Boehm, Phys. Rev. Lett. **98**, 167202 (2007).
  - <sup>14</sup> B. Thielemann *et al.*, Phys. Rev. Lett. **102**, 107204 (2009).
  - <sup>15</sup> T. Hong, Y. H. Kim, C. Hotta, Y. Takano, G. Tremelling, M. M. Turnbull, C. P. Landee, H. J. Kang, N. B. Christensen, K. Lefmann, K. P. Schmidt, G. S. Uhrig, and C. Broholm, Phys. Rev. Lett. **105**, 137207 (2010).
  - <sup>16</sup> D. Schmidiger, P. Bouillot, S. Mühlbauer, S. Gvasaliya, C. Kollath, T. Giamarchi, and A. Zheludev, Phys. Rev. Lett. **108**, 167201 (2012).
  - <sup>17</sup> A. A. Nersesyan, A. O. Gogolin, and F. H. L. Eßler, Phys. Rev. Lett. **81**, 910 (1998).
  - <sup>18</sup> T. Vekua and A. Honecker, Phys. Rev. B **73**, 214427 (2006).
  - <sup>19</sup> A. Lavarélo, G. Roux, and N. Lafforencie, Phys. Rev. B **84**, 144407 (2011).
  - <sup>20</sup> B. Koteswararao, S. Salunke, A. V. Mahajan, I. Dasgupta, and J. Bobroff, Phys. Rev. B **76**, 052402 (2007).
  - <sup>21</sup> O. Mentré, E. Janod, P. Rabu, M. Hennion, F. Leclercq-Hugéux, J. Kang, C. Lee, M. H. Whangbo, and S. Petit, Phys. Rev. B **80**, 180413 (2009).
  - <sup>22</sup> S. Wang, E. Pomjakushina, T. Shiroka, G. Deng, N. Nikseresht, C. Ruegg, H. Ronnow, and K. Conder, J. Cryst. Growth **313**, 51 (2010).
  - <sup>23</sup> O. Mentré, E. M. Ketatni, M. Colmont, M. Huvé, F. Abraham, and V. Petricek, J. Am. Chem. Soc. **126**, 10857 (2006).
  - <sup>24</sup> A. A. Tsirlin, I. Rousochatzakis, D. Kasinathan, O. Janson, R. Nath, F. Weickert, C. Geibel, A. M. Läuchli, and H. Rosner, Phys. Rev. B **82**, 144426 (2010).
  - <sup>25</sup> B. Koteswararao, A. V. Mahajan, L. K. Alexander, and J. Bobroff, J. Phys. Condens. Matter **22**, 035601 (2010).
  - <sup>26</sup> Y. Kohama, S. Wang, A. Uchida, K. Prsa, S. Zvyagin, Y. Skourski, R. D. McDonald, L. Balicas, H. M. Ronnow, C. Rüegg, and M. Jaime, Phys. Rev. Lett. **109**, 167204 (2012).
  - <sup>27</sup> B. Keimer, A. Aharony, A. Auerbach, R. J. Birgeneau, A. Cassanho, Y. Endoh, R. W. Erwin, M. A. Kastner, and G. Shirane, Phys. Rev. B **45**, 7430 (1992).
  - <sup>28</sup> B. Keimer, N. Belk, R. J. Birgeneau, A. Cassanho, C. Y. Chen, M. Greven, M. A. Kastner, A. Aharony, Y. Endoh, R. W. Erwin, and G. Shirane, Phys. Rev. B **46**, 14034 (1992).
  - <sup>29</sup> I. Dzyaloshinsky, J. Phys. Chem. Solids **4**, 241 (1958).
  - <sup>30</sup> T. Moriya, Phys. Rev. **120**, 91 (1960).
  - <sup>31</sup> I. Affleck and M. Oshikawa, Phys. Rev. B **60**, 1038 (1999).
  - <sup>32</sup> D. C. Dender, P. R. Hammar, D. H. Reich, C. Broholm, and G. Aeppli, Phys. Rev. Lett. **79**, 1750 (1997).
  - <sup>33</sup> M. Kenzelmann, Y. Chen, C. Broholm, D. H. Reich, and Y. Qiu, Phys. Rev. Lett. **93**, 017204 (2004).
  - <sup>34</sup> Y. J. Wang, F. H. L. Essler, M. Fabrizio, and A. A. Nersesyan, Phys. Rev. B **66**, 024412 (2002).
  - <sup>35</sup> C. Stock, W. J. L. Buyers, R. Liang, D. Peets, Z. Tun, D. Bonn, W. N. Hardy, and R. J. Birgeneau, Phys. Rev. B **69**, 014502 (2004).
  - <sup>36</sup> M. J. Cooper and R. Nathans, Acta. Cryst. **23**, 357 (1967).
  - <sup>37</sup> N. J. Chesser and J. D. Axe, Acta. Cryst. A **29**, 160 (1973).
  - <sup>38</sup> The high energy scattering is much broader than the resolution and does not disperse in the  $\mathbf{Q}$ -range probed. Since this intensity does not appear in scans performed at equivalent  $\mathbf{Q}$  positions in the  $(0, k, l)$  plane it is likely spurious scattering resulting from the coarse out-of-plane resolution of the vertically focusing monochromator.
  - <sup>39</sup> P. J. Brown, *International Tables for Crystallography*, Vol. C (Springer, Berlin, 2006) Chap. 4.4.5, pp. 454–461.
  - <sup>40</sup> K. Nomura, J. Phys. Soc. Jpn **72**, 476 (2003).
  - <sup>41</sup> P. C. Hohenberg and W. F. Brinkman, Phys. Rev. B **10**, 128 (1974).
  - <sup>42</sup> M. B. Stone, I. Zaliznyak, D. H. Reich, and C. Broholm, Phys. Rev. B **64**, 144405 (2001).
  - <sup>43</sup> S. Notbohm, P. Ribeiro, B. Lake, D. A. Tennant, K. P. Schmidt, G. S. Uhrig, C. Hess, R. Klingeler, G. Behr, B. Büchner, M. Reehuis, R. I. Bewley, C. D. Frost, P. Manuel, and R. S. Eccleston, Phys. Rev. Lett. **98**, 027403 (2007).
  - <sup>44</sup> B. Leuenberger, A. Stebler, H. U. Güdel, A. Furrer, R. Feile, and J. K. Kjems, Phys. Rev. B **30**, 6300 (1984).
  - <sup>45</sup> M. Matsuda, T. Yosihama, K. Kakurai, and G. Shirane, Phys. Rev. B **59**, 1060 (1999).
  - <sup>46</sup> G. Xu, C. Broholm, D. H. Reich, and M. A. Adams, Phys. Rev. Lett. **84**, 4465 (2000).
  - <sup>47</sup> K. Damle and S. Sachdev, Phys. Rev. B **57**, 8307 (1998).
  - <sup>48</sup> A. Zheludev, V. O. Garlea, L. P. Regnault, H. Manaka, A. Tsvelik, and J. H. Chung, Phys. Rev. Lett. **100**, 157204 (2008).
  - <sup>49</sup> B. Náfrádi, T. Keller, H. Manaka, A. Zheludev, and B. Keimer, Phys. Rev. Lett. **106**, 177202 (2011).
  - <sup>50</sup> A. Zheludev, S. E. Nagler, S. M. Shapiro, L. K. Chou, D. R. Talham, and M. W. Meisel, Phys. Rev. B **53**, 15004 (1996).
  - <sup>51</sup> M. Kenzelmann, R. A. Cowley, W. J. L. Buyers, and D. F. McMorrow, Phys. Rev. B **63**, 134417 (2001).
  - <sup>52</sup> G. Xu, C. Broholm, Y.-A. Soh, G. Aeppli, J. F. DiTusa, Y. Chen, M. Kenzelmann, C. D. Frost, T. Ito, K. Oka, and H. Takagi, Science **317**, 1049 (2007).
  - <sup>53</sup> T. Masuda, A. Zheludev, A. Bush, M. Markina, and

- A. Vasiliev, .
- <sup>54</sup> T. Masuda, A. Zheludev, B. Roessli, A. Bush, M. Markina, and A. Vasiliev, Phys. Rev. B **72**, 014405 (2005).
- <sup>55</sup> F. Damay, C. Martin, V. Hardy, A. Maignan, C. Stock, and S. Petit, Phys. Rev. B **84**, 020402 (2011).
- <sup>56</sup> V. O. Garlea, A. Zheludev, L. P. Regnault, J. H. Chung, Y. Qiu, M. Boehm, K. Habicht, and M. Meissner, Phys. Rev. Lett. **100**, 037206 (2008).
- <sup>57</sup> S. Miyahara, J. B. Fouet, S. R. Manmana, R. M. Noack, H. Mayaffre, I. Sheikin, C. Berthier, and F. Mila, Phys. Rev. B **75**, 184402 (2007).